Enhanced electrocatalytic nitrate-to-ammonia conversion performance from Ag-doped Co_3O_4 nanofibers

Bingyan Shi,[a] MingZe Xia,[a] Ruikai Qi,[a] YuMei Yang[b] and Xiaofeng Lu*[,a]

[a]*Alan G. MacDiarmid Institute, College of Chemistry, Jilin University, Changchun, 130012, P. R. China*

[b]*State Key Laboratory of Supramolecular Structure and Materials, College of Chemistry, Jilin University, Changchun 130012, P. R. China.*

E–mail address: xflu@jlu.edu.cn (Lu, X.)

*Corresponding author.

1. Experimental section

1.1. Chemicals

Polyacrylonitrile (PAN, M_w=150,000 g mol^{-1}) and poly(vinylpyrrolidone) (PVP, M_w=1,300,000 g mol^{-1}) were obtained from Sigma-Aldrich and Alfa Aesar, respectively. Ethanol (EtOH) was purchased from Beijing Chemical Works. Silver nitrate ($AgNO_3$) was procured from Shanghai Chemical Reagent Co., Ltd. Nafion solution was acquired from Shanghai Hesen Electric Co., Ltd. N, N-dimethylformamide (DMF) and cobalt acetate tetrahydrate ($Co(Ac)_2{\cdot}4H_2O$) were acquired from Sinopharm Chemical Reagent Co., Ltd. All chemicals were used without further purification.

1.2. Preparation of Ag-Co_3O_4 NFs

Specifically, a homogeneous solution was prepared by dissolving PVP (0.015 g), PAN (0.135 g), $AgNO_3$ and $Co(Ac)_2{\cdot}4H_2O$ (the total mass is 0.18 g) in 3 mL of DMF under continuous stirring overnight. The flexible $AgNO_3$/$Co(Ac)_2$/PAN/PVP precursor nanofibrous membrane was then fabricated by electrospinning the precursor solution. A stationary collector was placed 20 cm from the needle tip, with a solution flow rate of 0.45 mL min^{-1} and an applied voltage of 16 kV. The as-spun pale pink membrane was then calcined in a muffle furnace at 700 °C for 2 h in air, with a heating rate of 2 °C min^{-1}. This process yielded the final Ag/Co_3O_4 nanofibers, which turned black and transformed from flexible to a friable solid. The molar percentage of Ag was chosen as 5%, 10% and 15% (denoted as 5% Ag-Co_3O_4 NFs, 10% Ag-Co_3O_4 NFs, 5% Ag-Co_3O_4 NFs, respectively) by adjusting the contents of $AgNO_3$ and $Co(Ac)_2{\cdot}4H_2O$ in precursor solution. The bare Co_3O_4 NFs were synthesized without the addition of $AgNO_3$ during the preparation of electrospun precursor solution.

1.3. Characterization

The morphology of the sample was visualized using scanning electron microscopy (SEM, FEI Nova Nano SEM) measurement. Transmission electron microscopy (TEM, JEOL JEM-2100 F), high-resolution TEM (HRTEM, FEI Tecnai G2 F20) with elemental mapping and energy dispersive X-ray (EDX) spectroscopy were used to characterize the microscopic and crystal structure as well as the element distribution.

Powder X-ray diffraction (XRD, PANalytical B.V.) and Raman spectroscopy (LabRAM HR Evolution spectrometer, 532 nm excitation) were employed to reveal the chemical structure. X-ray photoelectron spectroscopy (XPS, Thermo Scientific Nexsa) confirmed the elemental valence states. The reaction products were quantified by ultraviolet-visible (UV-vis) spectrophotometer (Shimadzu UV-2501PC). ^{1}H-NMR spectroscopy was conducted on an Avance NEO NMR spectrometer operating at 400 MHz.

1.4. Electrochemical measurements

Electrochemical performance was rigorously validated using CHI 660E and CHI 760E electrochemical workstations with an H-type electrolytic cell (Hg/HgO and Ag/AgCl as reference electrode, Pt wire as counter electrode). The working electrode was prepared by the deposition of 10% Ag-Co_3O_4 NFs with 2% Nafion solution onto the carbon paper electrode with a mass loading of 1 mg cm^{-2}. The H-cell configuration comprised an anode compartment filled with 35 mL of 1.0 M KOH and a cathode compartment containing 35 mL of 1.0 M KOH + 0.1 M KNO_3 (or 0.5 M K_2SO_4 + 0.1 M KNO_3). Linear sweep voltammetry (LSV) curves were recorded at 5 mV s^{-1} from –0.6 to –2.0 V *vs.* Hg/HgO (or Ag/AgCl) electrode, with potentials converted to reversible hydrogen electrode (RHE). Unless otherwise stated, LSV curves are *iR*-compensated with the following equation. $E_{corrected} = E_{measured} - i \times R_s \times 90\%$, Cyclic voltammetry (CV) curves at scanning rates of 20–100 mV s^{-1} (0.3-0.4 V *vs.* Hg/HgO) were used for electrochemical double–layer capacitance (C_{dl}) determination. Electrochemical impedance spectroscopy (EIS) via Nyquist plots were acquired at –1.3 V *vs.* Hg/HgO (or Ag/AgCl) electrode with an amplitude of 0.005 V.

1.5. Assembly of the zinc-nitrate battery and electrochemical test.

The carbon paper (1 cm^2) loaded with 1 mg cm^{-2} of 10%Ag–Co_3O_4 and 0.25 mg cm^{-2} of carbon black and Zn sheet (1 cm^2) were employed as the cathode and anode for zinc-nitrate battery, respectively. A typical H-type cell that contains 30-mL cathode electrolyte (1 M KOH + 0.1 M KNO_3) and 30-mL anode electrolyte (3 M KOH) separated by Nafion117. The discharging polarization curves with a scan rate of 5 mV s^{-1} and galvanostatic tests were conducted using CHI 760E workstation at room

temperature, respectively.

1.6. Detection of NH_3

NH_3 quantification was performed via Nessler's reagent colorimetry. Following chronoamperometry tests, electrolyte aliquots were diluted to 4 mL, treated with 0.08 mL of potassium iodide solution (for enhancing the Nessler's reactivity) and 0.08 mL of Nessler's reagent, then analyzed by UV-vis spectrophotometry at 420 nm. NH_3 concentrations were determined from the measured absorbance using a standard calibration curve.

The NH_3 yield rate was calculated according to: $$Yield\ rate_{NH_3} = \frac{c_{NH_3} \times V}{t \times S}$$

The NH_3 Faradaic efficiency (FE) was calculated as follows:

$$FE_{NH_3} = \frac{8 \times F \times c_{NH_3} \times V}{M_{NH_3} \times Q}$$

where c_{NH3} is the mass concentration of NH_3 (aq), V represents cathode compartment electrolyte volume (35mL or 100 mL), M_{NH3} denotes the molar mass of NH_3, t signifies the electrolysis time (1 h, 2 h or 5 h), S corresponds to the geometric area of working electrode (0.2 cm^2), F is the Faradaic constant (96485 C mol^{-1}), Q indicates the total charge transferred during electrolysis.

1.7. Detection of NO_2^-

NO_2^- quantification was conducted using a colorimetric reagent comprising 0.4 g of *p*–aminobenzenesulfonamide, 0.02 g of N–(1–Naphthyl) ethylenediamine dihydrochloride,), 1 mL of phosphoric acid (density: 1.70 g/mL) in 29 mL of ultrapure water.

Post chronoamperometry, precise electrolyte aliquots were diluted to a total volume of 4 mL. After adding 0.08 mL of the colorimetric reagent, the absorbance of the resultant mixture was measured at 540 nm using a UV–vis spectrophotometer. NO_2^- concentrations were determined through interpolation on a pre–calibrated standard curve.

The FE for NO_2^- generation is calculated using the following methodology:

$$FE_{NO_2^-} = \frac{2 \times F \times c_{NO_2^-} \times V}{M_{NO_2^-} \times Q}$$

where c_{NO2-} denotes the mass concentration of NO_2^- (aq), V represents the cathode compartment electrolyte volume (35 mL or 100 mL), M_{NO2-} is the molar mass of NO_2^-, F signifies the Faradaic constant (96485 C mol^{-1}), Q indicates the total charge transferred during electrolysis.

1.8. Detection of NO_3^-

Post-chronoamperometry, the electrolyte was diluted and treated sequentially with HCl and amino sulfonic acid to eliminate nitrite interference. UV-vis spectrophotometry was then used to measure the solution absorbance at 220 nm and 275 nm. The NO_3^- concentration was determined by applying the absorbance difference ($A = A_{220\ nm} - 2A_{275\ nm}$) by comparing it to a calibration curve.

1.9. Isotope labeling experiments

Isotopic tracing of NH_3 was performed using 99.21% $K^{15}NO_3$ as the nitrogen source. The chronoamperometry test was conducted 1.0 M KOH with 0.1 M $K^{15}NO_3$. Post-electrolysis, the pH of the electrolyte was adjusted to a slightly acidic level with the addition of HCl. Thereafter, 0.05 mL of hexadeuterodimethyl sulfoxide (DMSO–d6) and 0.08 wt% maleic acid ($C_4H_4O_4$) were added into 0.4 mL of the diluted electrolyte.

1.10. Density functional theory (DFT) calculation

We performed DFT calculations using the Vienna Ab initio Simulation Package (VASP). The Perdew–Burke–Ernzerhof (PBE) functional under the generalized gradient approximation (GGA) was adopted for the exchange-correlation term. The core-valence electron interaction was modeled with projector augmented wave (PAW) potentials, and a plane-wave cutoff energy of 520 eV was used. Structural relaxations continued until all atomic forces were below 0.03 eV·$Å^{-1}$, and the self-consistent field calculations converged at an energy threshold of 10^{-6} eV. A vacuum layer exceeding 20 Å was included in the z-direction to separate periodic replicas.

The Gibbs free energy change (ΔG) for each step of the nitrate reduction reaction (NO_3RR) was determined using the standard thermodynamic expression:

$\Delta G = \Delta E + \Delta ZPE - T\Delta S$

where ΔE, ΔZPE, T (298.15 K), and ΔS correspond to the DFT total energy difference, zero-point energy correction, temperature, and entropy change, respectively. Data extraction and analysis were facilitated by the VASPKIT toolkit.

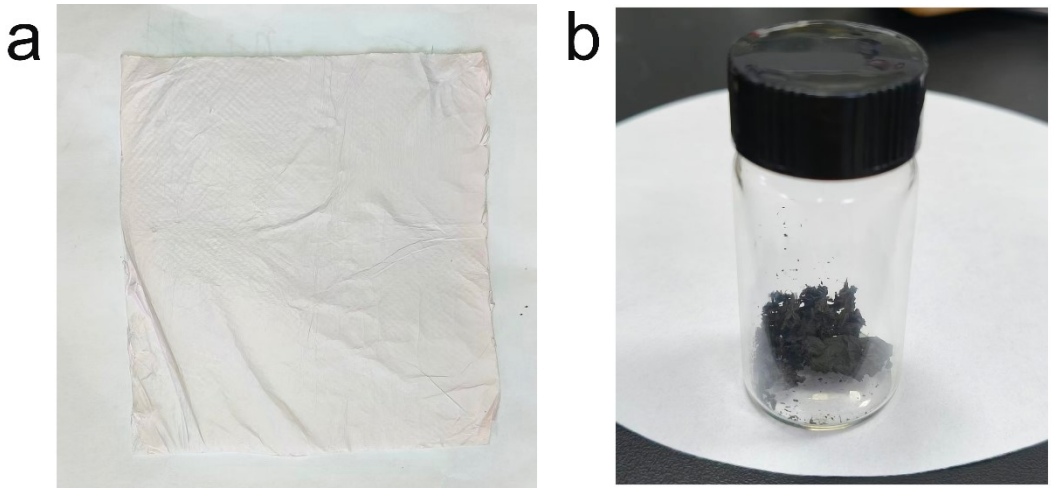

Fig. S1 The photographs of (a) $AgNO_3/Co(Ac)_2$/PAN/PVP precursor nanofibrous membrane and (b) its calcined product of Ag-Co_3O_4 NFs.

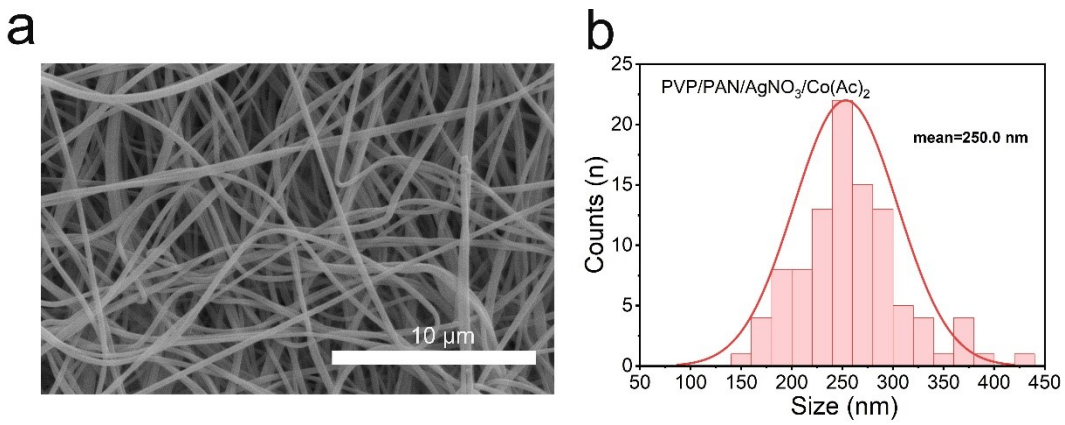

Fig. S2 (a) SEM image and (b) diameter distribution of PVP/PAN/$AgNO_3$/$Co(Ac)_2$ precursor nanofibers.

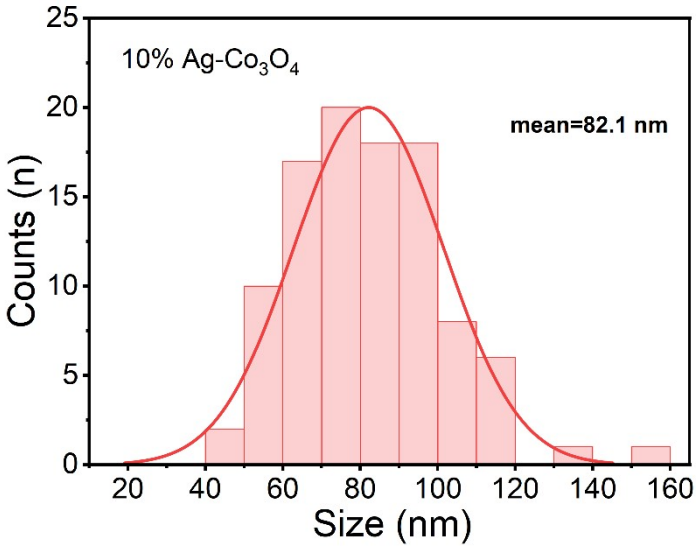

Fig. S3 Diameter distribution of 10% Ag-Co_3O_4 NFs.

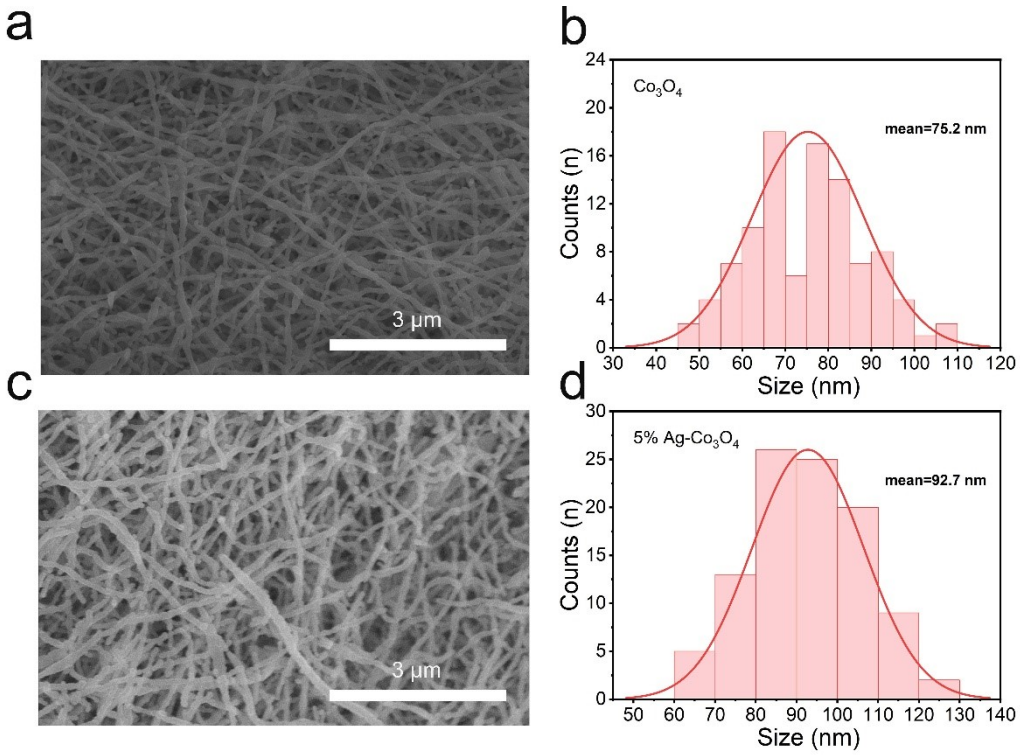

Fig. S4 SEM images and diameter distributions of (a, b) Co_3O_4 NFs and (c, d) 5% Ag-Co_3O_4 NFs.

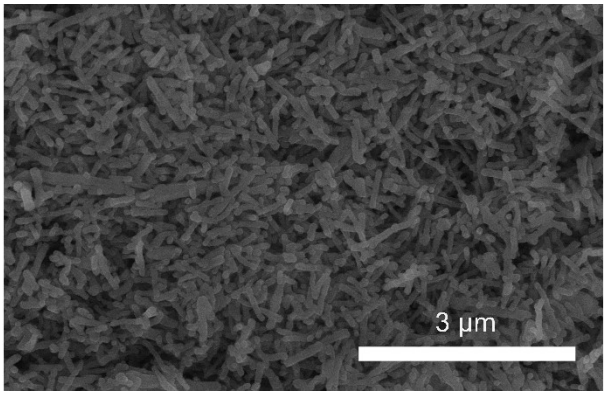

Fig. S5 SEM image of 15% Ag-Co_3O_4 NFs.

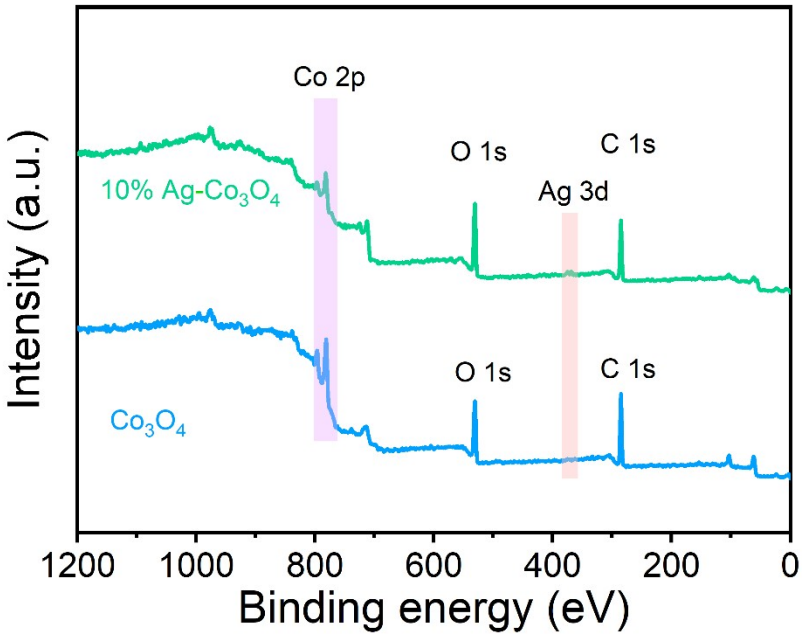

Fig. S6 XPS survey spectra of 10% Ag-Co_3O_4 NFs and Co_3O_4 NFs.

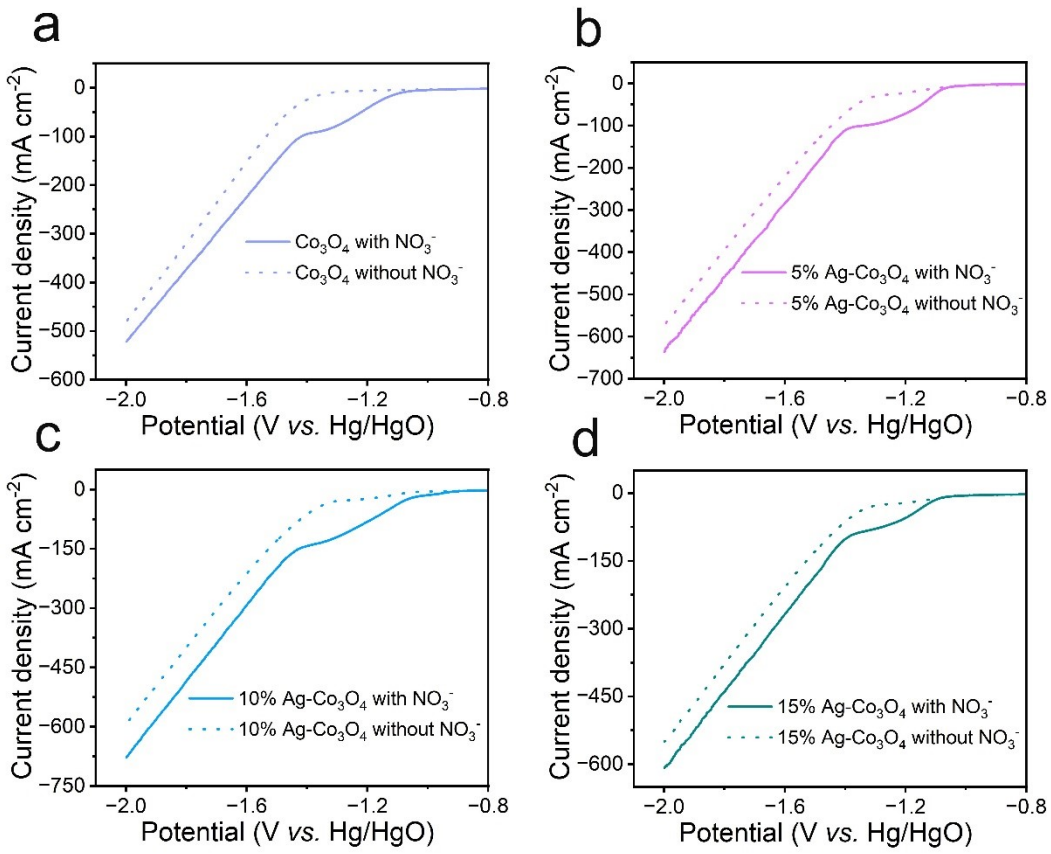

Fig. S7 LSV curves of (a) Co_3O_4 NFs, (b) 5% Ag-Co_3O_4 NFs, (c) 10% Ag-Co_3O_4 NFs and (d) 15% Ag–Co_3O_4 NFs in 1 M KOH with and without 0.1 M KNO_3 at scan rate of 5 mV s^{-1} without *iR*–compensation.

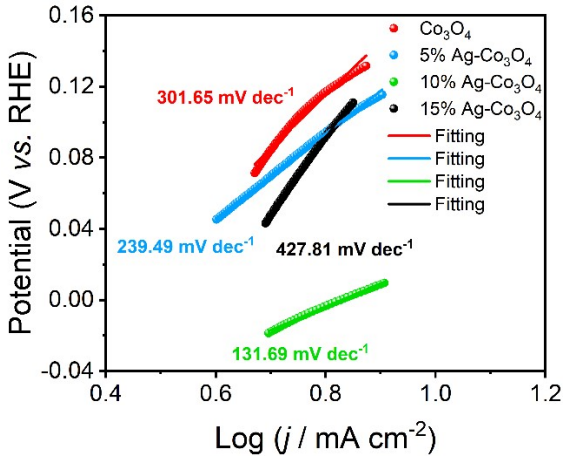

Fig. S8 Tafel plots for different catalysts.

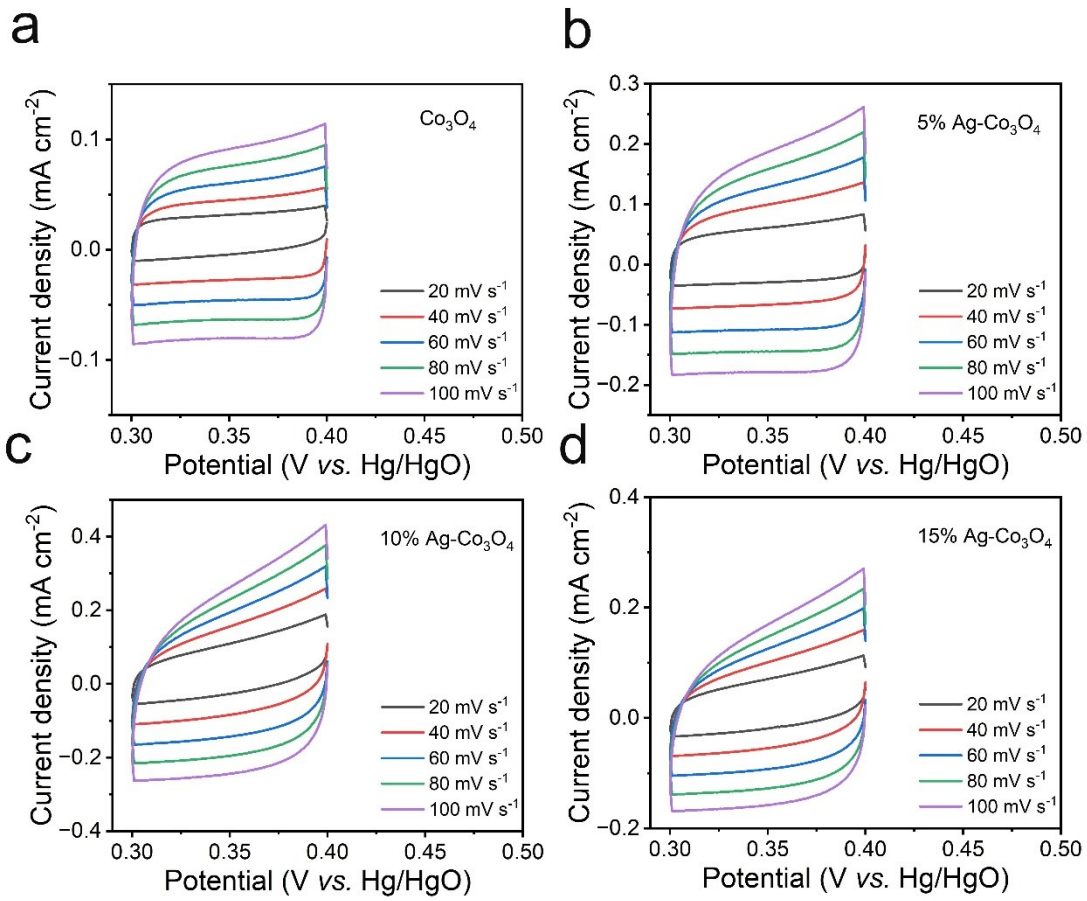

Fig. S9 CV for the determination of the C_{dl} for different samples. (a) Co_3O_4 NFs, (b) 5% Ag–Co_3O_4 NFs, (c) 10% Ag-Co_3O_4 NFs and (d) 15% Ag–Co_3O_4 NFs.

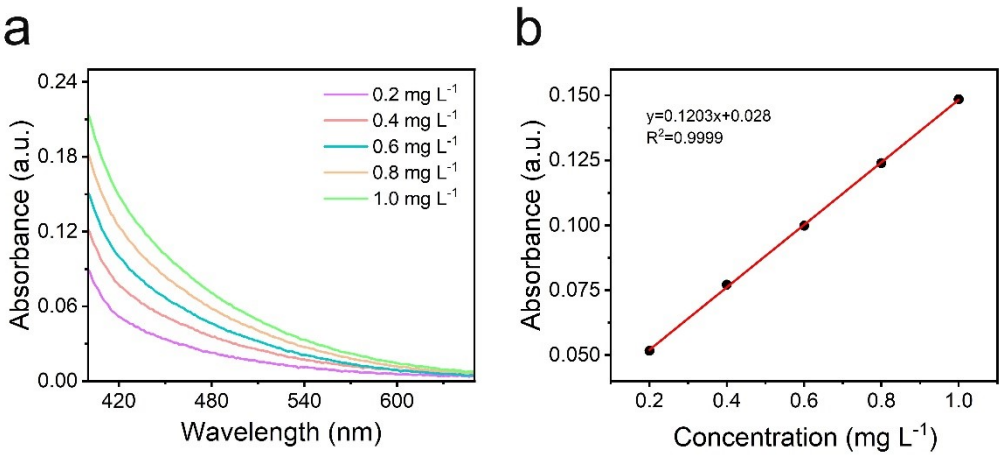

Fig. S10 (a) The UV-vis absorption and (b) concentration-absorbance calibration curve of NH_3–N.

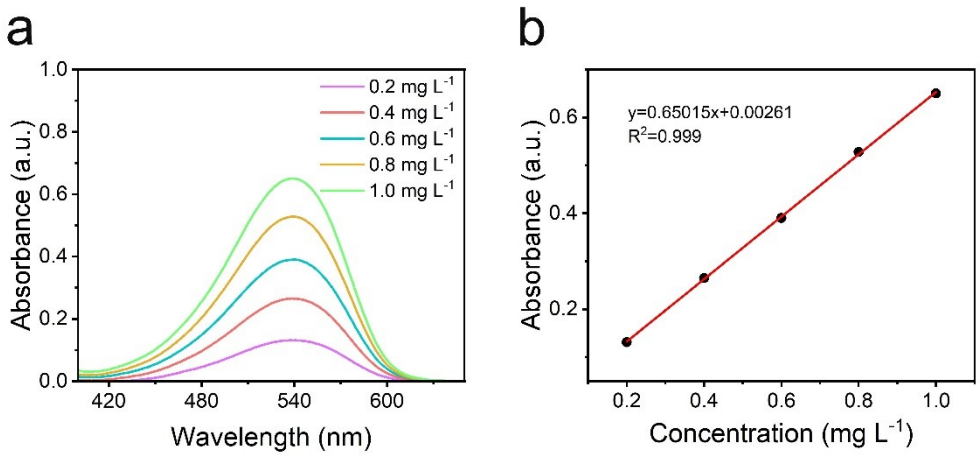

Fig. S11 (a) The UV-vis absorption and (b) concentration-absorbance calibration curve of NO_2^-–N.

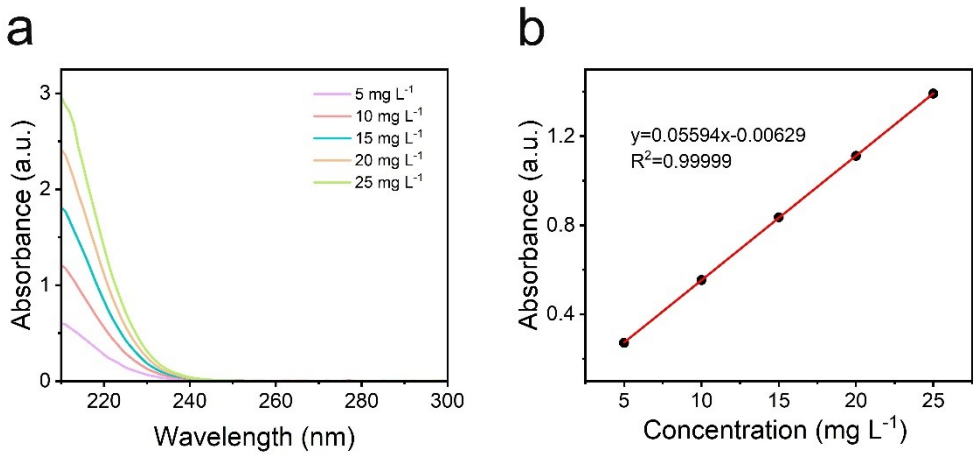

Fig. S12 (a) UV-vis absorption and (b) concentration-absorbance calibration curve of NO_3^-–N.

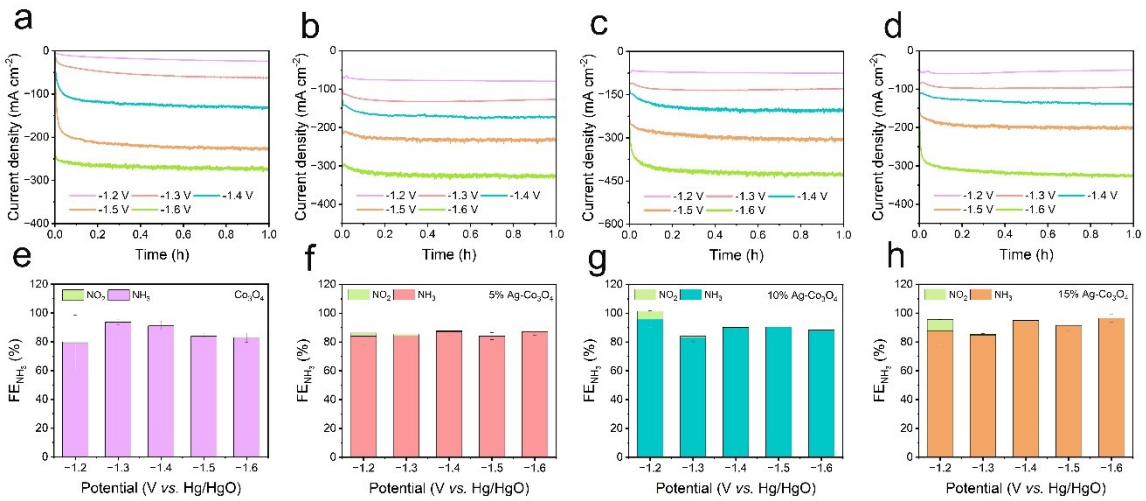

Fig. S13 Chronoamperometry curves of (a) Co_3O_4 NFs, (b) 5% Ag-Co_3O_4 NFs, (c) 10% Ag-Co_3O_4 NFs and (d) 15% Ag-Co_3O_4 NFs at different potentials for 1 h in 1.0 M KOH with 0.1 M KNO_3. The corresponding FE of NH_3 and NO_2^- for (e) Co_3O_4 NFs, (f) 5% Ag-Co_3O_4 NFs, (g) 10% Ag-Co_3O_4 NFs and (h) 15% Ag-Co_3O_4 NFs.

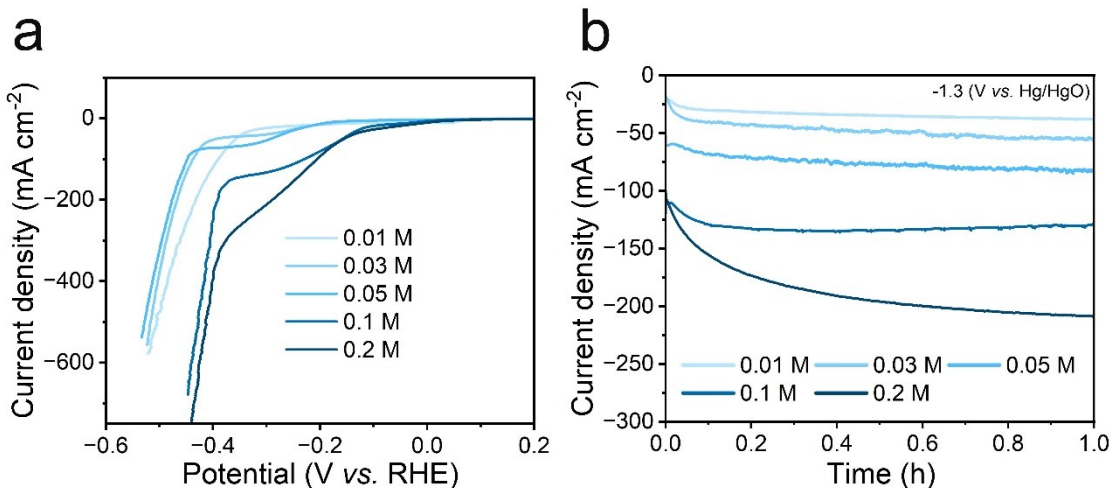

Fig. S14 (a) LSV plots of 10% Ag-Co_3O_4 NFs for NO_3RR in 1 M KOH containing various concentrations of KNO_3 from 0.01 to 0.2 M with 90% *iR*-compensation. (b) Chronoamperometry curves of 10% Ag-Co_3O_4 NFs under different concentration of KNO_3 at the potential of –1.3 V *vs.* Hg/HgO.

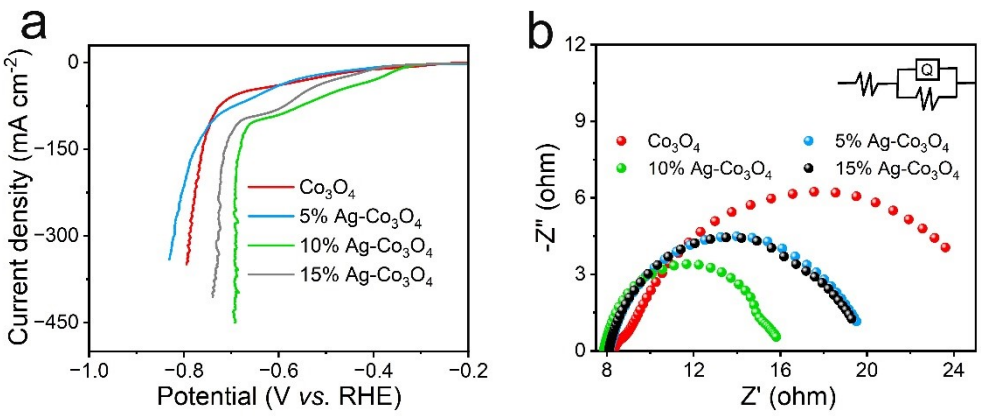

Fig. S15 NO_3RR performance of varied catalysts in 0.5 M K_2SO_4 with 0.1 M KNO_3 electrolyte. (a) The 90% *iR*-compensated LSV curves of different catalysts. (b) The Nyquist plots of different catalysts at the potential of –1.3 V *vs.* Ag/AgCl electrode (inset: equivalent circuit model).

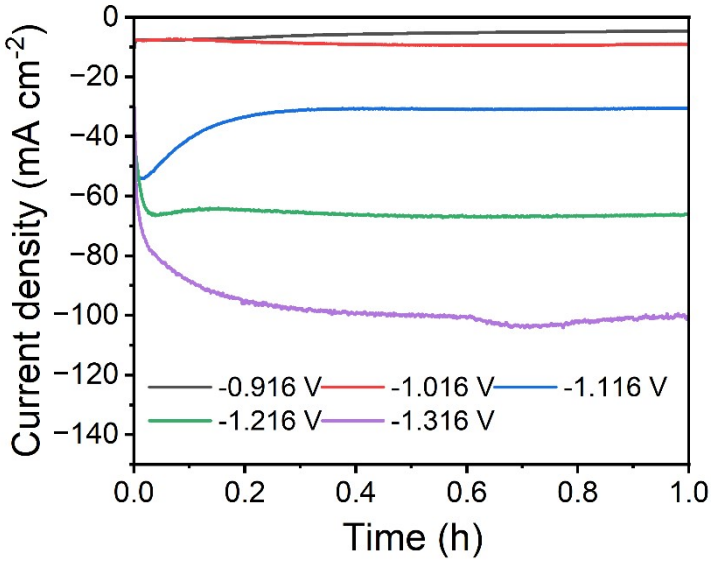

Fig. S16 Chronoamperometry curves of 10% Ag-Co_3O_4 NFs in 0.5 M K_2SO_4 with 0.1 M KNO_3 (potential *vs.* Ag/AgCl).

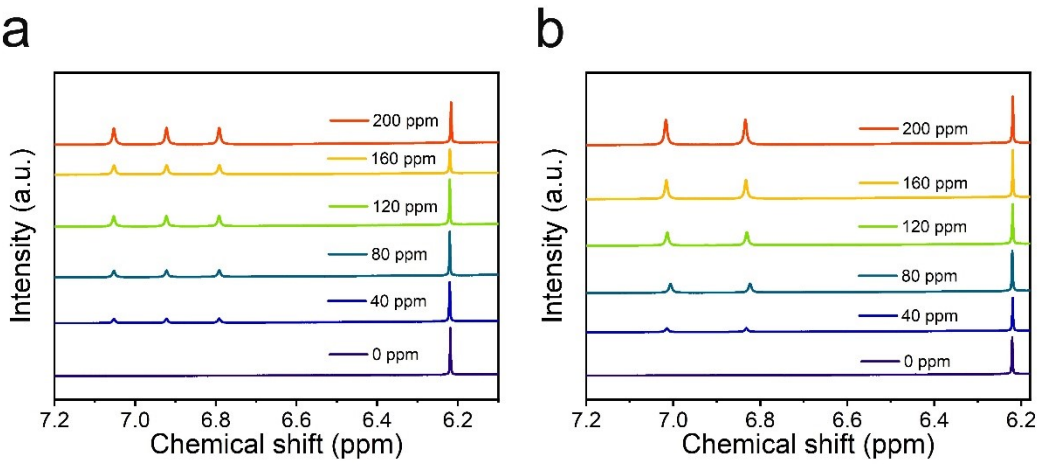

Fig. S17 (a) ^{1}H-NMR spectra of $^{14}NH_4Cl$ and (b) $^{15}NH_4Cl$ with different concentrations. NMR spectra of the products produced after the electrocatalytic NO_3RR of 10% Ag-Co_3O_4 NFs in the electrolyte of 1 M KOH with 0.1 M $K^{14}NO_3$ or $K^{15}NO_3$ at –0.675 V *vs.* RHE.

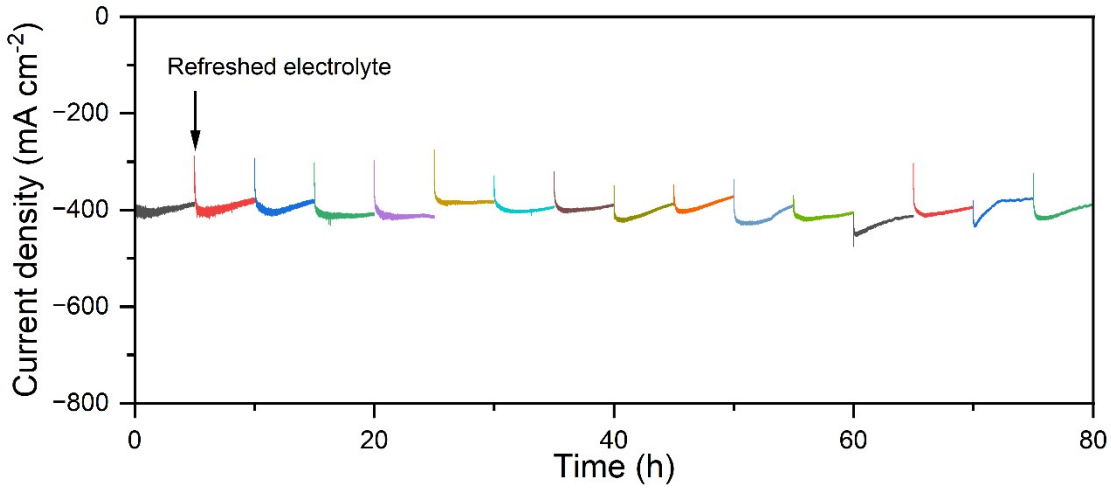

Fig. S18 Chronoamperometric curves of 10% Ag-Co_3O_4 NFs at –0.675 V *vs.* RHE in 1 M KOH with 0.1 M KNO_3 by 16 cycles, and each cycle presents 5 h of long-term electrolysis.

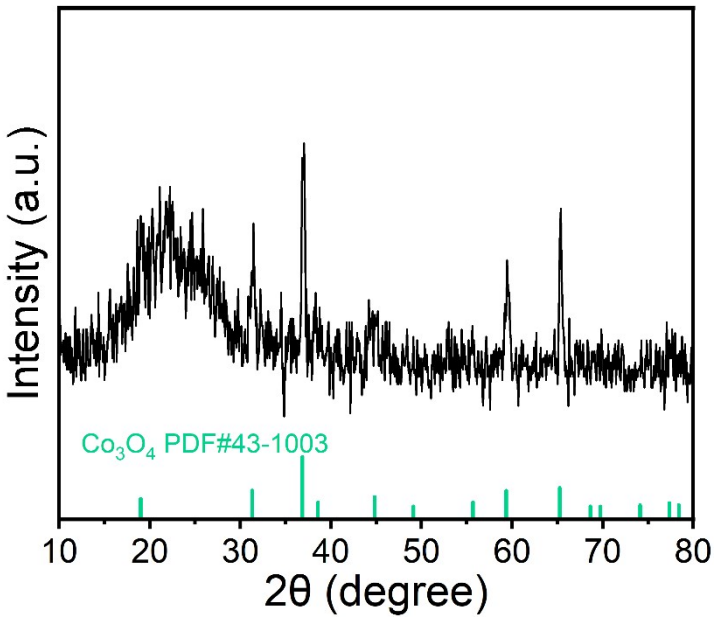

Fig. S19 XRD pattern of 10% Ag-Co_3O_4 NFs after chronoamperometric measurement.

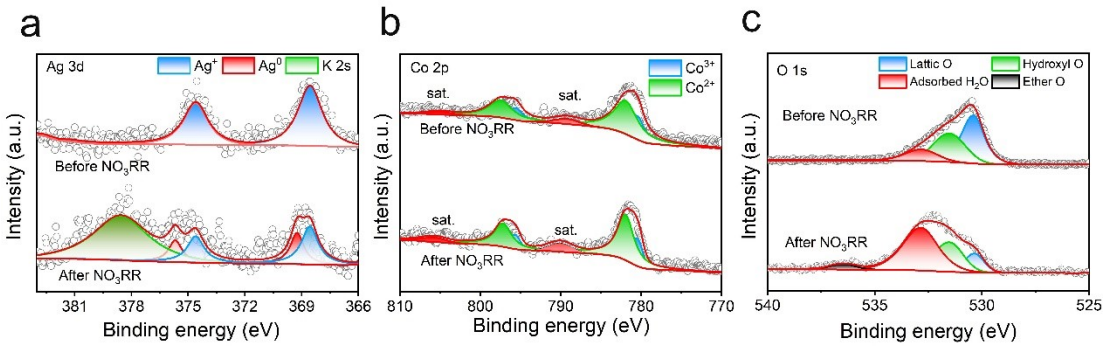

Fig. S20 (a) Ag 3d, (b) Co 2p and (c) O 1s XPS spectra of 10% Ag-Co_3O_4 NFs before and after NO_3RR process.

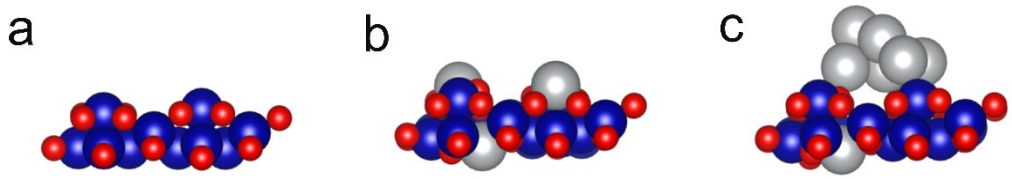

Fig. S21 Steady-state model configurations of (a) Co_3O_4, (b) Ag-Co_3O_4-1 and (c) Ag-Co_3O_4-2 from tope side view used in this work.

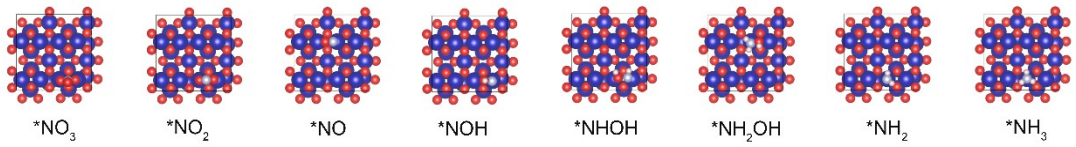

Fig. S22 The adsorption configurations of various intermediates on the Co_3O_4.

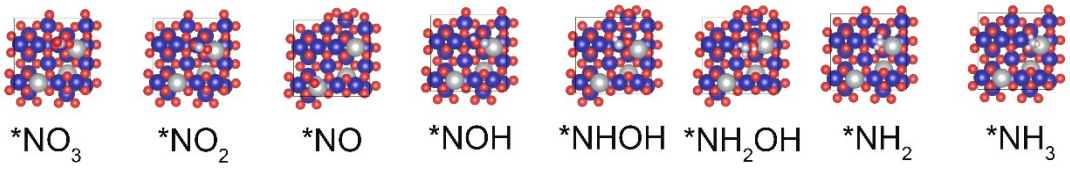

Fig. S23 The adsorption configurations of various intermediates on the Ag-Co_3O_4-1.

Table S1. Molar percentage of Co and Ag for the metals in different samples.

Catalysts	Co (mol%)	Ag (mol%)
5% Ag-Co_3O_4 NFs	95.5	4.5
10% Ag-Co_3O_4 NFs	90.4	9.6
15% Ag-Co_3O_4 NFs	85.6	14.4

Table S2. The C_{dl} and ECSA values from the relationship between capacitive current density and different scan rates.

Samples	C_{dl} (mF cm^{-2})	ECSA (cm^2)
Co_3O_4 NFs	0.84	4.2
5% Ag-Co_3O_4 NFs	1.63	8.15
10% Ag-Co_3O_4 NFs	2.14	10.7
15% Ag-Co_3O_4 NFs	1.37	6.85

Table S3. Comparison of the NH_3 yield rate of 10% Ag-Co_3O_4 NFs with other catalysts reported

Catalysts	Electrolyte	NH_3 yield rate (Potential, *vs.* RHE)	Reference
10% Ag-Co_3O_4 NFs	1 M KOH 0.1 M KNO_3	29.11818 mg cm^{-2} h^{-1} –0.675 V	This work
MP-Cu	1 M KOH with 0.05 M NO_3^-	0.543 mmol h^{-1} cm^2 –0.5 V	Adv. Funct. Mater. 2023, 33, 2212236
Co_2NiO_4	0.5 M Na_2SO_4+0.1 M KNO_3	20 mg cm^{-2} h^{-1} –1 V	Appl. Catal. B Environ. 2024, 340, 123219
Ag-Co_3O_4	0.1 M KOH 0.1 M KNO_3	1.2741 mg cm^{-2} h^{-1} –0.42V	ACS Catal. 2024, 14, 15, 11231–11242
Cu_2O@CoO	1 M KOH 0.1 M KNO_3	15.27 mg cm^{-2} h^{-1} –0.9V	ACS Nano 2024, 18, 31, 20258–20267
Co/NCD@Co(OH)$_2$	1 M $NaNO_3$ + 1 M NaOH	5.73 mol h−1 m^{-2} at −0.3 V vs. RHE	Chem. Commun., 2025, 61, 3203–3206
$(Cu_{0.6}Co_{0.4})Co_2O_4$	1 M KOH 0.1 M KNO_3	1.09 mmol h^{-1} cm^{-2} at −0.45 V	J. Am. Chem. Soc. 2024, 146, 2967–2976
CoP NAs/CFC	0.1 M ph–CH_2OH + 1 M $NaNO_3$+ 1 M NaOH	9.56 mol h^{-1} m^{-2}–0.3 V *vs.* RHE	Energy Environ. Sci., 2022, 15, 760–770
Cu–NSs	10 mM NO_3^- 0.1 M KOH	390.1 μg cm^{-2} h^{-1} –0.15 V	Appl. Mater. Today, 2020, 19, 100620
Cu_2Cl_2(BINAP)$_2$	0.5 M K_2SO_4+0.1 M KNO_3	373.0 μmol h^{-1} cm^{-2} –0.946 V	Angew. Chem. Int. Ed. 2024, 64, e202413033
Bi_1–$CuCo_2O_4$	0.5 M Na_2SO_4+0.1 M KNO_3	448.74 μmol h^{-1} cm^{-2} –0.8 V	Adv. Funct. Mater. 2024, 34, 2409696
Cu_xCo_yHHTP	0.5 M Na_2SO_4+0.1 KNO_3	299.9 μmol h^{-1} cm^{-2} –0.6 V	Chem. Eng. J., 2023, 466, 1385
CoP NWAs/NF-300	0.2 M K_2SO_4 100 ppm KNO_3	110.4 μmol h^{-1} cm^{-2} –0.7 V	Chem. Eng. J., 2023, 474, 145546
Pd-Co_3O_4/TM	0.1 M NaOH (0.1 M NO_3^-)	528.74 μmol h^{-1} cm^{-2} –0.6 V	Small, 2023, 19, 2303424

Fe single atom	0.50 M KNO_3, 0.10 M K_2SO_4	0.46 mmol h^{-1} cm^{-2} –0.85 V	Nat. Commun., 2021, 12, 2870
Cu@C	1× 10^{-3} M NO_3^-	469.5 μg h^{-1} cm^{-2} –0.9 V	Adv. Mater., 2022, 34, 2204306

Table S4. Comparison of power density, OCV and NH_3 yield rate between 10% Ag-Co_3O_4 and recently reported cathodes in Zn-NO_3^- battery.

Catalysts	Electrolyte	NH_3 yield rate (mg cm^{-2} h^{-1})	OCV (V)	Power density (mW cm^{-2})	Reference
10% Ag–Co_3O_4	3 M KOH|| 1 M KOH +0.1 M KNO_3	1.32	1.34	7.20	This work
Cu_1/ZnO	\	1.2597	1.51	5.5	J. Am. Chem. Soc. 2025, 147, 737−18746
Ni-MOF-Ru	3 KOH||6 M KOH + 1 M KNO_3	2.1008	1.42	4.99	ACS Catal. 2024, 14, 16205–16213
Co_1Zn NSs	\\||1 M KOH + 0.2M KNO_3	1.7102	1.39	5.1	Angew. Chem. Int. Ed. 2026, 65, e23740
Cu-N_4	6 M KOH with 0.2 M $Zn(Ac)_2$||1 M KOH + 0.1 M $NaNO_3$	0.468	1.26	7.18	Adv. Funct. Mater. 2025, 35, 2501057
$FeCo_2O_4$@ $CuCo_2O_4$/CF/ PTFE	\	0.6273	1.67	6.47	Appl. Catal. B Environ. Energy 2025, 365, 124899
$Cu_3(HHTP)_2$/CF	6 KOH+0.2 M $Zn(Ac)_2$||1 M KOH + 0.1 M $NaNO_3$	0.468	1.26	7.18	Adv. Funct. Mater. 2025, 35, 2501057
Cu_2O/$Cu(OH)_2$@$Ni(OH)_2$	\	2.78	1.37	6.47	Adv. Sci. 2026, 13, e21252
Ir SAC Co_3O_4	6 KOH||0.1 M NaOH +	0.7633	1.393	5.6	Chem. Catal. 2023, 3,

	0.1 M NO_3^-				100477.
NiCoBDC@ HsGDY	6 KOH||0.1 M NaOH +0.1 M NO_3^-	1.125	1.47	3.66	ACS Nano 2023, 17, 6687.